Biol Cell (1992) 74, 43–50

Review

Scanning secondary ion analytical microscopy with parallel detection

Georges Slodzian [1], Bernard Daigne [2], François Girard [2], Fabrice Boust [2], François Hillion [3]

[1] *Laboratoire de Physique des Solides, Bât 510, Université Paris-Sud, 91405 Orsay;* [2] *ONERA, BP no 72, 92320 Châtillon;* [3] *CAMECA 103, bld Saint-Denis, 92400 Courbevoie, France*

(Received and accepted 13 December 1991)

Summary – The secondary ion microscope described here allows to obtain the simultaneous registration of chemical and isotopic distribution maps of several elements composing the sample. The instrument has been specially designed to optimize both sensitivity and selectivity: bombardment with primary Cs^+ ions to increase the ionization yields of negative secondary ions, efficient collection of secondary ions at the target surface, matching of the secondary ion beam etendue with the acceptance of the mass spectrometer working at high mass resolution, spectrometer with parallel detection capabilities. The probe diameter can be made as low as 30 nm and ion induced electron images registered at the same time as ion images. Presently, four ion micrographs are obtained simultaneously over a field of view up to 20 × 20 μm^2 containing up to 512 × 512 pixels. Examples are shown with an ion probe diameter of 0.1 μm.

secondary ion mass spectrometry / high resolution ion microscopy / parallel detection of different ionic species / high mass resolution spectrometer

Introduction

Any mass spectrometric method used to analyze solid samples is a destructive technique, *ie* target atoms have to be ejected and ionized to produce a characteristic signal. For example, Ia is a typical ion related to an element A in the sample, getting a signal made of a number N (Ia) of Ia ions implying the destruction of a given microvolume. Now, as in any type of microscopy, the aim is to bring down the lateral resolving limit which here means to make as small as possible the size of the microvolume which must be sputtered to produce the information contained in each pixel of the ion micrograph, recalling that secondary ion emission has the potential of sampling the target down to microvolumes in the range of 10^{-6} μm^3 for each pixel. Then, the basic problem is to build an instrument having not only the capability to resolve small details but also a sensitivity high enough to obtain an adequate signal out of each sputtered microvolume. Let us briefly recall the main factors influencing the size of this microvolume.

First, the sputtered microvolume contains a number K of target atoms which comprise different atomic (or isotopic) species A, B, ... with atomic concentrations CA, CB, ... In any practical case, one will have to compare signals related to different elements. With a conventional mass spectrometer, the ionic species are successively registered while the sputtering of the target is going on. As a consequence, if the dwell time on each spectral line is the same, the size of the minimum microvolume is multiplied by a factor equal to the number of elements. Obviously, the microvolume needed for an analysis would be minimized if a parallel detection system would be used for the different ionic species.

The useful yield τ is the other important factor. By definition, τ^{-1} is the mean number of atoms A that must be removed from the sample to detect one ion Ia. To obtain a number N(Ia) of characteristic ions Ia, it is necessary to sputter a microvolume (in μm^3) in the order of $[N(Ia)/\rho\tau CA]$ where ρ is the atomic density (in atoms/μm^3). As long as the size of the collision cascades can be neglected, the magnitude of this volume sets a limit to the spatial resolution.

The useful yield depends upon: i) the efficiency of the ionisation processes; ii) the overall transmission of the instrument (ratio of the number of the ions being produced to the number of ions reaching the detector); and iii) the quantum efficiency of the detector. The design of the instrument must also take into account the existence of various cluster ions possessing the same number of atomic mass units. Thus, the spectrometer must have the capability of working at high mass resolving powers to bypass the confusion in mass identification and nevertheless have a high transmission.

The instrument described in this paper is a scanning ion microscope, using a cesium ion probe, coupled with a magnetic sector double focusing mass spectrometer possessing a straight focal plane. The instrument has been designed to achieve; i) high lateral resolving power; ii) high mass resolution with high transmission; iii) parallel detection for different ionic species [1, 2].

Basic considerations

Scanning microscope versus direct microscope

The first applications of secondary ion emission in biology have used direct imaging microscopy and most present studies are still going on using this technique [3]. In a direct imaging instrument, the primary beam illuminates a broad area and the sputtered ions, stemming from each point of the bombarded surface, are focused into an image by an immersion objective lens. Each image point is surrounded by an aberration disk which limits the lateral resolution in the ion micrograph. The size of the aberration disk can be reduced by limiting the angular aperture

of the pencil of ions trajectories converging in each image point with a material stop placed on the crossover of the objective lens. This operation results in a lowering of the signal, that is a reduction of τ, which may become redhibitory when one aims at low lateral resolving limits. However, direct imaging is very convenient for surveying a sample in the range of 1 μm resolving limit because the ion image is displayed on a fluorescent screen almost instantaneously.

On the other hand, in a scanning microscope, the lateral resolving limit is obtained by focusing the primary beam into a small spot of the sample surface and the size of this spot sets the resolving limit. As a consequence, there is no limitation of the collection efficiency of secondary ions by lateral resolving limit requirements. Then, another type of limitation appears due to the fact that secondary ions are emitted with a broad energy spectrum and a large angular distribution. Indeed, those energy and angular initial distributions determine the etendue of the secondary ion beam which contains most of the emitted intensity originating in the probe area. Since this etendue does not fit, in general, what the spectrometer will accept for a given mass resolving power, new stopping down of the secondary beam is necessary. Nevertheless, the useful yield is expected to be much higher in the case of a scanning microscope coupled to a mass spectrometer.

Acquisition time

In a scanning microscope, the ion microprobe is rastered over the sample surface and the acquisition time t_a for an ion picture depends upon the dwell time t_d in each pixel and upon the number $N \times N$ of pixels in the picture. If we neglect the time necessary to switch from one pixel to the next, $t_a = t_d N^2$. The number N(Ia) of secondary ions per pixel is a function of the total sputtering yield Y, the useful yield τ, the intensity I_p in the probe, the atomic concentration CA and the dwell time t_d per pixel:

$$N(Ia) = Y\ CA\ \tau\ I_p\ t_d$$

Let us take a spectrometer permanently tuned on the ionic species Ia and let us try 'reasonable' values for the previous parameters so as to evaluate what can be expected. With $\tau \approx 10^{-2}$, Y $\approx$ 4 (target atoms)/(primary ion) $I_p \approx 10^7$ ions/s (1.6 pA), CA $\approx 10^{-2}$ and t_d = 8 ms, the following numbers are obtained $n_p = I_p t_d \approx 8 \times 10^4$ (primary ions)/pixel, $N_t \approx 3.2 \times 10^5$ (sputtered target atoms)/pixel, N(Ia) = 32 ions/pixel that is 4×10^3 counts/s and $t_a \approx$ 8.75 mn for a picture with 256 $\times$ 256 pixels.

Let us now consider the situation where the previous ion signal is ten times smaller either because the useful yield τ or because the concentration CA is smaller. If a Poisson distribution is assumed to be valid, a mean counting number of 3.2 would give a probability of about 96% to obtain at least one count per pixel. Thus, in the absence of any background, such an ion signal would still be adequate to ascertain the presence of element A in a given area of the sample.

With fixed values of τ, CA and Y, the only way to improve the counting statistics in the situation just described would be to increase the number N_p of primary ions striking each pixel. This can always be done by increasing t_d and consequently the acquisition time. In the example taken here, to reach the previous counting statistics of 32 ions/pixel would require to multiply t_a by a factor of ten. In other words it would take about 1.5 h to register the ion micrograph. It is a long time and can be used only in exceptional cases. Of course, it would be much simpler to increase the intensity I_p carried by the probe but, depending upon the diameter of the probe, this operation might go beyond the capabilities of the instrument. The acquisition time is not the only parameter to be considered as the two previous situations are compared. Indeed, if the ion signal is divided by ten, ten times more atoms have to be sputtered in order to obtain the same time integrated signal per pixel.

The evaluations made until now are valid whatever the probe size (except for the point that it might not be possible to increase I_p for small probe diameters). If this new parameter is taken into account, it is easy to figure out that, with a 1-μm probe in the first of the two situations being considered, obtaining 32 counts/pixel would require the sputtering of 2% of a monolayer whereas with a 0.1-μm probe it would take about two monolayers. Thus, there is a change from static to dynamic SIMS conditions. Clearly for small probes and/or lower signals, several monolayers will have to be consumed in most cases so that, in general, we will have to deal with dynamic SIMS conditions in high resolution ion microscopy.

Choice of the nature of primary ions and ion source

In static SIMS conditions, the ionization probability depends upon the surface chemistry. The same is true in dynamic SIMS conditions but now the chemical state of the surface results from the dynamics of sputtering, implantation of primary ions, bombardment induced diffusions or induced surface reactions with the vacuum gas phase. By bombarding the sample with reactive ions, it is often possible to change the surface chemistry in a direction which favors the increase of the useful yield.

In this work, Cs^+ primary ions have been chosen to enhance the useful yield of negative secondary ions [4, 5]. For example, τ for oxygen O^- ions sputtered from a silica sample is sixty times higher when the sample is bombarded with cesium ions than with argon ions. It should also be noted that about one-third of the periodic table is composed of elements having an electron affinity high enough for producing negative ions with good yields. In less favorable cases, elements may form clusters with high affinities. For instance, AlO (3.6 eV) or CN (3.82 eV) have affinities of the same order as that of chlorine (3.6 eV).

The yield of negative ions depends upon the concentration of cesium implanted in the upper atomic layers of the target. When the bombardment is started on a fresh surface, the yield varies as a function of time before a dynamic equilibrium is reached in which the removal of implanted cesium atoms by sputtering occurs at the same rate as the rate of arrival of primary ions. As an example, after the onset of the beam, the intensity of $^{12}C^-$ ions emitted from a fresh carbon surface exhibits a sharp decrease first, goes through a minimum and then gradually increases up to a stationary value two orders of magnitude higher than the minimum: what appears as a sharp decrease is due to the removal of chemisorbed layers (part of the secondary emission used in static SIMS), the minimum corresponds to the emission of carbon target not yet significantly loaded in cesium and the progressive increase, up to the saturation level, expresses the increase of implanted cesium concentration in the target upper layers. The time scale of this evolution depends upon the primary density and the whole process takes the sputtering of about a few tens of nanometers before reaching the steady state.

It should also be noted that the amplitude of the increase due to cesium implantation varies from one element to another according to its electron affinity. Indeed, if an element has a high affinity one may expect that its ion yield will be high right from the beginning of the bombardment so that the enhancement due to cesium implantation will be modest (much less than 10 for CN^-). On the contrary, an element with low electron affinity will exhibit a strong increase of its ionic yield because the starting level is low. This is likely to explain some of the results published on the comparison of gallium and cesium bombardments [6]. Besides, the atomic concentration of cesium in the upper layers depends upon the sputtering yield of the target, therefore, the yield of a given element may vary according to the matrix.

Naturally, other primary ions can be used to produce similar enhancement effects. It is well known that the implantation of oxygen or halogen ions has a strong influence on the production of positive secondary ions. The choice of cesium ions will be completed with other reactive primary ions in the future.

As has already been stated, the intensity carried by the probe should be the highest possible to lower the acquisition times. For cesium primary ions, there was the choice between liquid metal and thermal ionization sources. In the present stage of instrument development, the latter has been preferred even though the probes are produced with lower currents. The source presently used is of a special design which is described elsewhere [7]. It provides us with a beam of 10 keV energy possessing a small crossover (40 μm), a thermal energy spread (< 1 eV), a reasonable brightness (150 A/cm^2/Sr), good operation stability (better than 0.5% over 10 mn) and no manipulation of liquid cesium.

Choice of the mass spectrometer

Parallel detection can be achieved in several ways. A time of flight (TOF) spectrometer would be, in many respects, the ideal instrument [8]. Unfortunately, the duty cycle is too small (10^{-4}) so that it would take too long to obtain ion micrographs with 256 × 256 pixels. The solution actually experimented with is made of a combination of electrostatic and magnetic sector fields. The layout is similar to a Mattauch-Herzog instrument since the mass spectrum is displayed along a focal plane. The problem is then to have a parallel detection system possessing both high sensitivity and enough spatial resolution along the focal plane, *ie* a modern version of the photographic plate without its well known inconveniences. A provisional solution has been designed consisting of discrete detectors placed at adjustable positions along the focal plane. This solution allows us to choose detectors having a large dynamical range since one deals with signals ranging from a few 10^6 counts/s to less than one count/s. Other experimental arrangements for special situations can be planned but no universal satisfactory solution has been found as yet.

Description of the instrument

Co-axial probe forming and ion collecting optical system

The same optical set is used to focus the primary beam into a fine spot on the sample and to collect the secondary ions. The schematic diagram of this objective lens

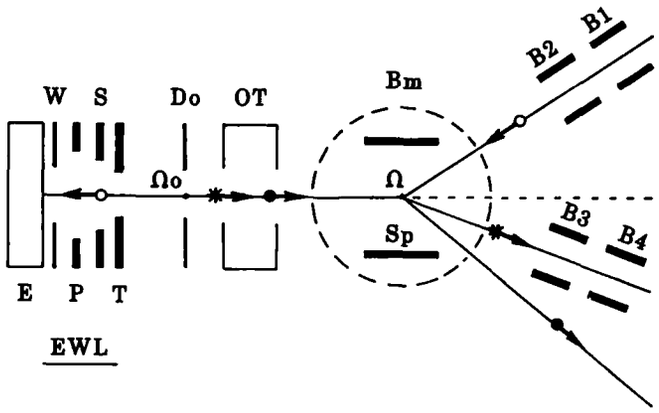

Fig 1. Co-axial objective lens EWL and separation of the beams: Primary ions (o), secondary ions (*) and electrons (•). Bm magnetic field for separating secondary electrons.

EWL is shown in figure 1. The first electrode is the target itself which is a plane conducting surface polarized at a negative voltage (−5 kV). It is followed by four electrodes W, P, S and T with revolving symmetry about an optic axis perpendicular to the surface target: W is at the same voltage as the target, P and S are at positive and negative voltages respectively and T is at ground potential. Primary and secondary ions have different energy and opposite signs, thus P mainly acts upon the primary positive ions and S on the secondary negative ions which makes the adjustments for each type of particles almost independent.

At the surface of the target, secondary ions experience a strong electrostatic field (about 20 kV/cm) which counteracts the natural dispersion of the trajectories resulting from the angular and energy dispersion of ejected particles. This feature contributes to minimize loss in the subsequent transport of the beam. Besides, the last demagnifying lens of the probe forming system has the smallest possible working distance so that its chromatic and spherical aberration coefficients (22 mm and 38 mm respectively) are small which is favorable for producing probes with high current density.

The diaphragm, Do, adjustable both in position and size, controls the aperture of the primary beam (and thus the aberrations on the probe). The position of Do along the optic axis has been chosen to coincide with the image plane of the sample surface produced by EWL with secondary ions. As a result, the size of Do limits the area from which secondary ions can be collected. Do is large enough to leave the collection efficiency of secondary ions unaltered over a square sample area of several tens of micrometers side.

Separation of the primary and secondary beams and scanning scheme

After EWL, the transport of the primary and secondary ion beams along the same axis is achieved by an optical system (OT) as well as the transport of the beam of secondary electrons emitted under the impact of primary ions. The beams are deviated by the action of crossed electrostatic and magnetic fields inside Sp. The electrostatic field acts on the positive primary and negative secondary particles with forces in opposite directions and produces deviations with different amplitudes because the energy is not the same. In addition, the magnetic field splits the secondary beams into its ionic and electronic components.

The electron beam is directed towards a scintillator associated with a photomultiplier. The amplified signal is numbered after an amplitude to frequency conversion and is used to produce an electronic image of the surface. This ion → electron image is extremely useful for adjusting the focus of the probe and for surveying the sample (fig 4).

The secondary ion beam is directed towards the spectrometer through a transport system, not described here, which, in addition, produces a shaping of the beam so as to improve the transmission of the spectrometer.

The two sets of scanning plates B1 and B2 (fig 1) act on the primary ions only and make their beam rotate about the center Ω of Sp. The system (OT) conjugates Ω with the center Ωo of the diaphragm Do so that the diaphragm limits a solid angle always made of the same type of primary rays.

The two sets of deviating plates B3 and B4 act only on the secondary ion beam. They are powered in synchronism with the scanning of the primary beam so as to maintain the axis of the secondary beam in a fixed position when the ion probe is moved on the sample surface. This procedure allows us to have the same transmission for the spectrometer when the primary beam is rastered over the whole field of view, in other words, there is no 'vignetting' on the ion micrographs when the overall transmission is maximum.

Mass spectrometer and detection system

The considerations presented above have guided our choice of the spectrometer. We have designed a mass spectrometer made of an association of two sectors (electrostatic EP and magnetic MP) coupled with a quadrupole lens, Q, and a slit lens, SL, and possessing a focal plane, FP, along which the different ionic species are focused as narrow lines (fig 2). It is an instrument which provides us with angular and energy-first-order focusing all along the focal plane for trajectories in the so-called 'horizontal section' which is the plane of symmetry chosen for the drawing in figure 2. Additional features improve the transmission at high mass resolution (correction of second order aperture aberrations by a proper choice of the entrance, exit and deviation angles of the magnetic prism and by the action of a hexapole, Hx, in front of the electrostatic sector, focusing in the vertical section by SL, etc) [1].

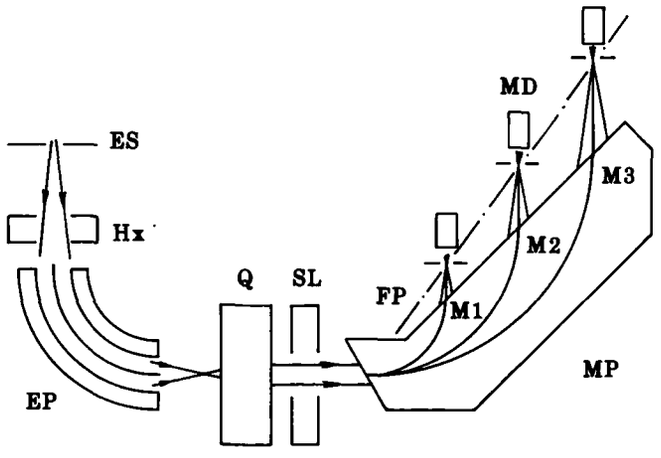

Fig 2. Schematic diagram of the double-focusing mass spectrometer with its focal plane FP. Three detection units are shown adjusted for three different ionic species M1, M2 and M3. ES is the entrance slit. For other items see text.

Several gears can be moved along the focal plane, each comprising a selection slit followed by an open electron multiplier magnetically shielded: a Faraday cup may replace the electron multiplier. Presently, four detection units are in operation moved by step-by-step motors under computer control. The open multipliers have been preferred to a channel plate stretched out along the focal plane [9] because their quantum efficiency is better and their dynamical range is larger since at high counting rates, with narrow lines covering only a few tens of channels, saturaton is likely to occur with channel plates.

The mass range that can be displayed along the focal plane is given by the interval (MO, ME) where MO and ME stand for the atomic masses of ions running, inside the magnet, along the shortest and the longest radii, respectively. In our present set-up ME = 20 × MO and MO can be varied from 1 to 50 by changing the strength of the magnetic field from 0.14 to 1 T.

With the miniature open multipliers being used here, the minimum distance between two adjacent slits is presently 9 mm which allows simultaneous detection of mass numbers differing by one unit up to mass number 19. This situation could be improved, for instance by blowing up a small fraction of the spectrum with an adequate projection optical system.

Instrument performances

Presently, four mass analyzed secondary ion micrographs and one electron picture can be recorded simultaneously. The number of pixels can be varied from 64 × 64 to 512 × 512. The probe is moved step by step, the dwell time per pixel can be adjusted from 1 to 64 ms and the time to switch from one pixel to the next is less than 2 μs. A computer-driven acquisition system stores count numbers from each pixel in the four selected ionic images. Distribution images related to different ionic species, in exact registration with each other, are produced from the same sputtered volume. Then, the $N \times N$ matrices stored in the memory can be used for various calculations and can be displayed on a CRT using 256 grey scale levels or different colour scales.

For a given probe diameter, the intensity can be optimized by a proper demagnification of the source and aperturing of the beam. In our instrument, we currently work with 0.1-μm probes carrying up to 3 pA. The probe diameter here is defined as the diameter d_p which contains 80% of the intensity. Smaller probes can also be produced as shown in the ion → electron micrograph (fig 3) obtained on a graphite sample: probe diameter 30 nm, 512 × 512 pixels, 10 × 10 μm^2 and $t_a \simeq 35$ mn.

The evaluation of the useful yield of $^{12}C^-$ on a graphite sample has given a value $\tau \simeq 5 \times 10^{-3}$ referring to the full intensity of the $^{12}C^-$ mass spectral line. A mass resolving power of 12 000 at FWHM or 6000 at 20% valley and 3000 at 2% valley between equal height peaks can be deduced from this line shape. For resolving powers lower than 1000, τ takes value of 4×10^{-2} which shows that there is still room for improving the transmission.

Examples showing the use of the microscope

SiC fibers embedded in a TA6V matrix

The sample is made of silicon carbide fibers embedded in a TA6V matrix (90% Ti, 6% Al, 4% V) [10]. Four micro-

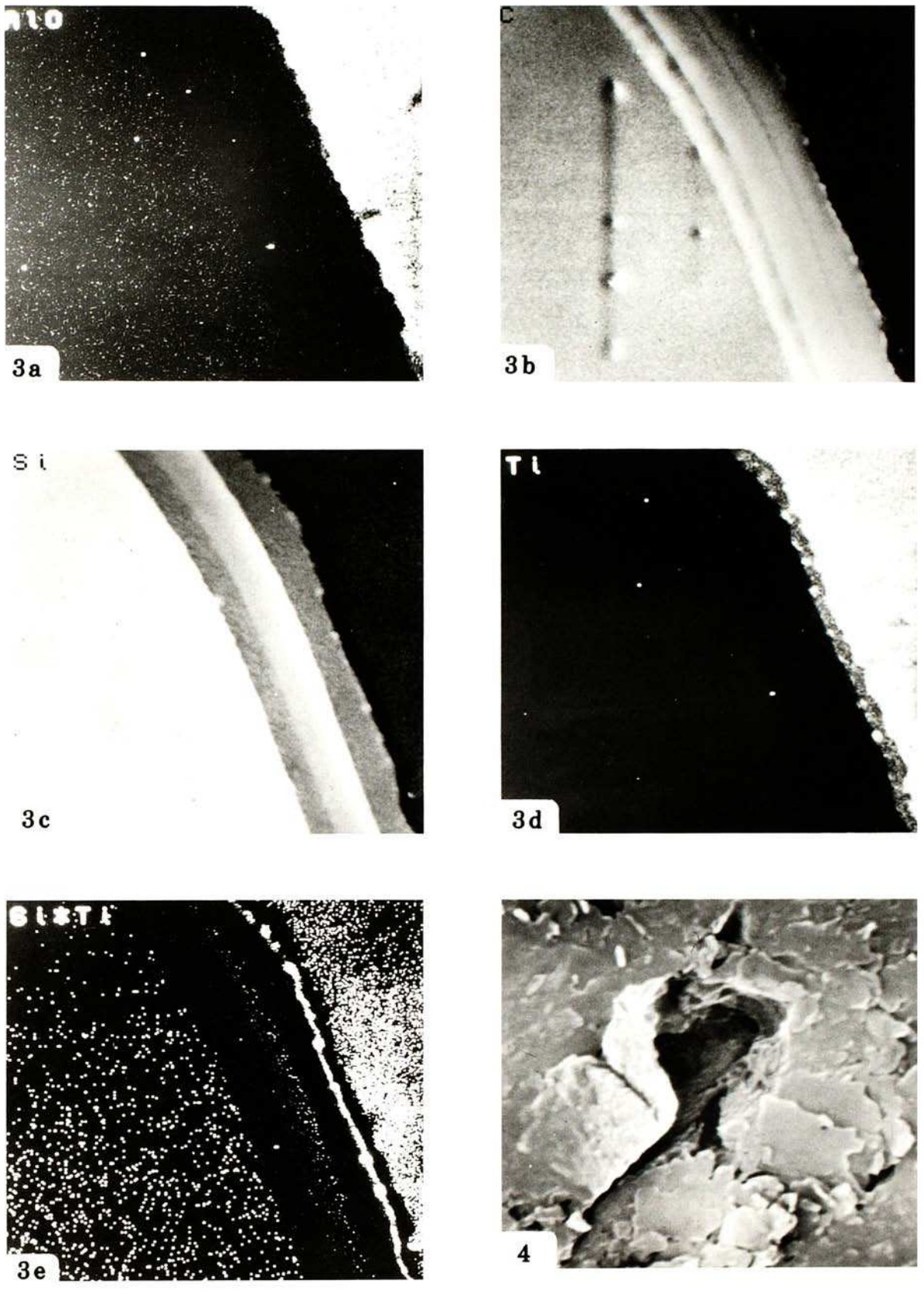

Fig 3. Simultaneous 15 × 15 μm^2 ion images on a SiC fiber embedded in a TA6V matrix: **a.** Al; **b.** C; **c.** Si; **d.** Ti and **e.** Ti*Si correlation image. Linear display between 1 and M ions/pixel in (**a**), (**b**), (**d**) and (**e**) with M respectively equal to 25, 940, 100 and 6 500. Logarithmic display (1, 2 500) in (**c**).

Fig 4. Graphite sample. Ion → electron image: 10 × 10 μm^2, $d_p \simeq 30$ nm.

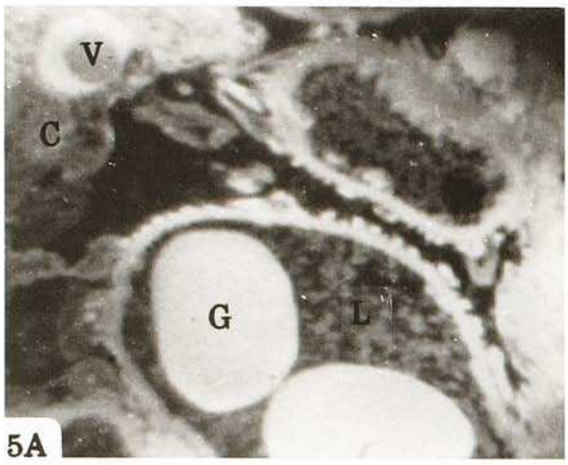

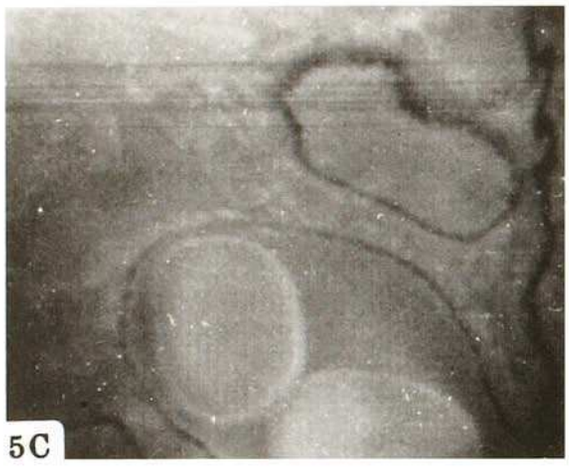

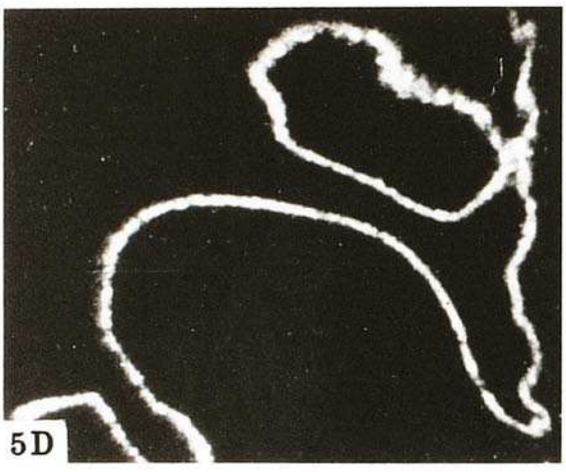

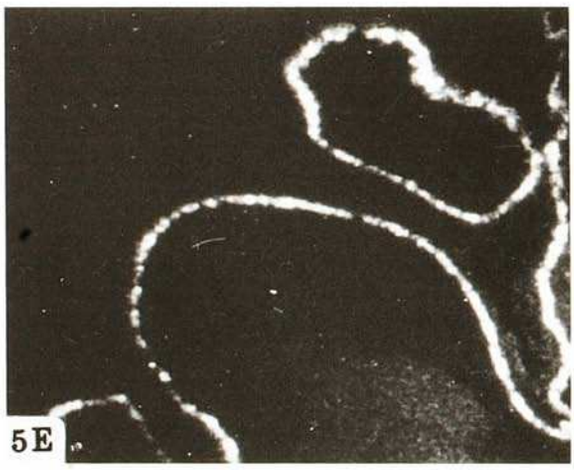

Fig 5. Chemical micrographs of an Epon section of a kidney glomerulus. Field of view 20 × 20 μm^2, 256 × 256 pixels. Probe diameter 0.1 μm. **A.** $^{12}C^{14}N^-$ linear display (0, 5000). **B.** $^{32}S^-$ square root display (0, 800). **C.** $^{12}C^-$ linear display (0, 2500). **D.** $^{107}Ag^-$ linear display (0,20). **E.** $^{80}Se^-$ linear display (0,15).

graphs simultaneously recorded on a polished section perpendicular to the fibers axes are shown in the interface region (fig 3). The Cs^+ probe diameter is $d_p \approx 0.1$ μm and carries 1 pA. The number of pixels is 256 × 256 for a field size of 15 μm × 15 μm. The counting time per pixel is 16 ms and the total acquisition time is a little more than 18 min. $^{12}C^-$, $^{28}Si^-$, $^{47}Ti^{18}O^-$ and $^{27}Al^{16}O^-$ secondary ions have been used. Aluminium and titanium having low electron affinities (0.44 eV and 0.08 eV, respectively), it turned out that the best sensitivity was obtained with AlO^- and TiO^- ions, the contribution of oxygen is likely to come from the chemisorbed vacuum gas phase (the residual pressure being about 10^{-7} mbar). The thickness of the layer which is eroded during the recording is in the range of a few nanometers. In each micrograph, the total number of counts is $^{12}C^- \rightarrow 2.6 \times 10^7$, $^{28}Si^- \rightarrow$

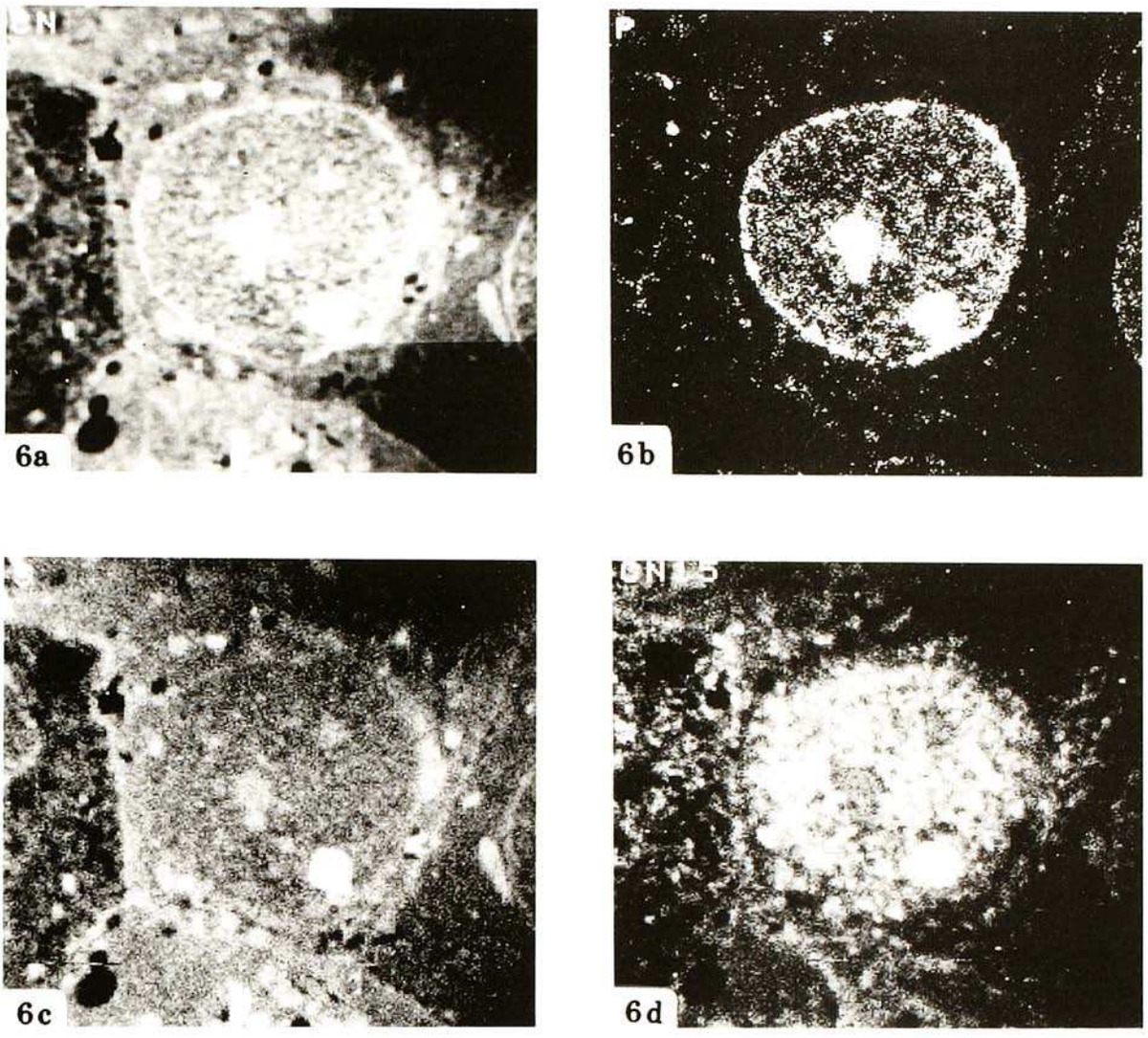

Fig 6. Labelled (^{15}N) adenine molecules traced in a human breast cancer cell. Pictures: 256 × 256 pixels in a 20 × 20 μm^2 field of views. Probe: $d_p \approx 0.1$ μm and $I_p \approx 1$pA. **a.** $^{12}C^{14}N^-$ logarithmic display (100, 3000) in counts pixel, total counts Ns ≈ 7.2 × 10^7. **b.** $^{31}P^-$ linear display (1, 25), Ns ≈ 2.5 × 10^5. **c.** $^{32}S^-$ linear display (1, 100), Ns ≈ 2.4 × 10^6. **d.** $^{12}C^{15}N^-$ linear scale (1, 100), Ns ≈ 1.6 × 10^6.

4.2 × 10^7, $^{27}Al^{16}O^-$ – 2.4 × 10^5 and $^{47}Ti^{16}O^-$ → 1.1 × 10^6.

In the interface region one can observe a variety of zones with different compositions. It is possible to correlate the presence of two elements pixel by pixel. For instance, the picture (fig 3e) has been built by multiplying, pixel by pixel, the number of counts in Si and in Ti and then suitably normalized. In this picture, a border line beaded with small precipitates, likely to be SiTi containing some carbon, can be demonstrated.

Elemental mapping in a kidney glomerulus

The micrographs in figure 5 show the chemical maps of five elements in an Epon section of a kidney glomerulus from a patient poisoned by silver. The 1-μm thick section, was placed on a flat metallic holder. The micrographs were obtained with a 0.1-μm probe and an acquisition time of 35 mn. The field of view, 20 × 20 μm^2 contains 256 × 256 pixels.

Pictures A and B, representing the distribution of nitrogen and sulphur, allow one to recognize the histological structure of a portion of glomerulus comprising: the lumen, L, of the capillaries, the red blood cells, G, the cytoplasm, C, of an epithelial cell with a vacuol, V, and its periphery rich in sulphur and nitrogen. Picture C shows that the distribution of carbon is spread rather homogeneously in the kidney tissue as well as in the inclusion medium except at the level of the capillary basement membranes which appear as darker lines. Micrographs D and E show the distribution maps of silver and selenium respectively and demonstrate that those elements are localized in the basement membranes, extracellular part of the capillary walls. Besides, it seems that the red blood cells contain some selenium.

Tracing labelled molecules in a human breast cancer cell

This example refers to a biological sample of a human breast cancer cell 24 h after the introduction of adenine

molecules labelled with ^{15}N stable nitrogen isotope in the culture medium [11]. The micrographs shown (fig 5) are obtained with 1-μm thick section tissue. Because of the proximity of the mass numbers the pictures have been simultaneously recorded two by two, $^{31}P^-$ with $^{12}C^{14}N^-$ and $^{32}S^-$ with $^{12}C^{15}N^-$, the acquisition time of each set is $t_a \simeq 35$ mn.

The $^{12}C^{14}N$ micrograph gives the general structure of the cell and the ^{31}P image, which is related to the presence of nucleic acids and the structure of the elemental mapping in a nucleus.

The ^{32}S micrograph, roughly speaking, represents the distribution of proteins more or less rich in sulphur. In this micrograph the arrows point towards three nucleoli, two of them appear bright in the ^{31}P image and the other as the weaker dot surrounded by a depleted area. The nucleoli can also be seen on the $^{12}C^{14}N$ micrograph.

Adenine is known to incorporate both in DNA and RNA. It can be observed in the $^{12}C^{15}N^-$ image that among the three nucleoli only one labelled molecules, demonstrating that in the same nucleus different nucleoli may be at different phases of RNA synthesis at a given time.

Conclusion

The scanning ion microscope described here in an experimental set-up aiming at high sensitivity and selectivity has allowed us to test the optical design, to survey possible applications, to evaluate a few essential parameters such as the useful yield, the mass resolving power, probe diameters (with their associate intensities) and to locate the features that have to be modified to improve the performances. In particular, the optical scheme could be made much simpler by suppressing the scanning electron microscope built inside the instrument along the axis of the co-axial objective and which has not been described here for the sake of simplicity. If, in addition, the sample voltage were increased from 5 to 10 kV, computer simulations show that the overall transmission could be improved at high mass resolution (the useful yield measurements on $^{12}C^-$ already mentioned show that secondary ionic signal is lost). Sub-micron probes and/or parallel detection instruments [8, 12–14] have already been described but here we have tried to realize a design consistent with the fact that the method is destructive which means that we have tried to use in a consistent way high yield ionization processes, efficient collection of secondary particles, parallel detection and high transmission at high mass resolution.

The parallel detection capabilities can still be developed but it seems difficult to reach the flexibility of the TOF spectrometer for surface analysis or heavy molecule identification. However, the use of a sector instrument is presently essential for imaging with small probes ($\simeq 0{,}1$ μm) because there are no duty cycle limitations since the mass channels are permanently open. Of course, this conclusion must be revised if one would limit the analysed area to a small number of pixels.

In heterogenous samples, when specific features have to be analysed (precipitates in metals, matrix-fiber interfaces, nucleoli or mitochondria in cells) obtaining the analytical information often requires the removal of a number K of target atoms much larger than that corresponding to a fraction of monolayer. In general, it will not be possible to rely on the chemical state of the surface as it comes out from the sample preparation to produce an adequate useful yield throughout the sputtering of a number of atoms equivalent to several monolayers. The bombardment with reactive primary ions (Cs^+, O^- is then one of the possible ways for changing the yields in a favorable direction and it is what has been realized here for the negative emission mode.

Acknowledgments

The authors are grateful to professor P Galle and his group for providing the biological samples and their help in the interpretation of the micrographs.

References

1 Slodzian G, Daigne B, Girard F, Boust F (1988) High sensitivity and high spatial resolution ion probe instrument. *Proceedings VI*th Int Conf on SIMS, Versailles, 1987, (Benninghoven A, ed) John Wiley, p 189

2 Slodzian G, Daigne B, Girard F, Boust F, Hillion F (1990) Cartographie parallèle de plusieurs éléments ou isotopes par balayage avec une sonde ionique submicronique: premiers résultats, *CR Acad Sci Paris*, 311, 57–64

3 SIMS microscopy in biological problems (1992) (Fragu P, ed) *Biol Cell* 74, Elsevier, Paris

4 Schuhmacher M, Migeon HN, Rasser B (1992) Comparative useful yield measurements under oxygen, gallium and cesium bombardment. *Proceedings VIII*th Int Conf on SIMS, Amsterdam, 1991, (Benninghoven A, ed), John Wiley

5 Storm HA, Stein JD, Brown FK (1976) ARL Probe news, Joint US/Japan Seminar on SIMS technique Honolulu

6 Bernheim M, Slodzian G (1982) Caesiated surfaces and negative ion emission. *Proceedings III*rd Int Conf on SIMS, Budapest 1981, (Benninghoven A, ed) Springer Verlag, p 151

7 Slodzian G, Daigne B, Girard F, Hillion F (1992) A high resolution scanning ion microscope with parallel detection of secondary ions. *Proceedings VIII*th Int Conf on SIMS, Amsterdam, 1991

8 Schwieters J, Cramer HG, Heller T, Jürgens U, Niehuis E (1991) High mass resolution surface imaging with a TOF-SIMS scanning microprobe (Zehnpfenning JF, Benninghoven A, eds) *J Vac Sci Technol*, in press

9 Nikei Y, Satoh H, Oward M (1990) Liquid metal ion microprobe studies using parallel ion detection. *VII*th *Int Conf on SIMS*, Monterey, 1989 (Benninghoven A, ed) John Wiley p 821

10 Lancin M, Anxionnaz F, Schumacher M, Dugne O, Trebbia P (1987) Analysis by SIMS and by EELS-EDX in a STEM of SiC fibres reinforced composites. *Adv Structural Ceramics Symp Boston, MA, USA* 1–3 Dec 1986. Pittsburgh, PA, USA: *Mat Res Soc*, Vol 78, 231–238

11 Hindie E, Slodzian G, Beaupain R, Daigne B, Girard F, Hillion F, Galle P (1992) High resolution intracellular mapping of nitrogen 15 labelled molecules. *Proc VIII*th *Int Conf on SIMS*, Amsterdam, 1991

12 Levi-Setti R, Grow G, Wang YL (1985) Progress in high resolution scanning ion microscopy and secondary ion mass spectrometry imaging microanalysis. *Scanning Electron Microsc*, II, 535–551

13 Waugh AR, Bayly AR, Anderson K (1984) SIMS with very high spatial resolution using liquid metal ion sources. *Proceedings IV*th *Int Conf on SIMS*, Osaka, 1983, (Benninghoven A, ed), Springer Verlag, 138

14 Schucler B, Saunder P, Reed DA (1990) A new time-of-flight secondary ion microscope. *Proceedings VII*th *Int Con on SIMS*, Montercy, 1989, (Benninghoven A, ed) John Wiley, p 851